AGU PUBLICATIONS

Geochemistry, Geophysics, Geosystems

RESEARCH ARTICLE

10.1002/2014GC005497

Key Points:
- Paleomagnetic results of the MBT in four loess sequences are synchronized
- Timing of the MBT in Chinese loess is estimated to be around 808–826 ka
- The MBT is older and longer in Chinese loess than in marine records

Correspondence to:
Y. Sun,
sunyb@ieecas.cn

Citation:
Zhao, H., X. Qiang, and Y. Sun (2014), Apparent timing and duration of the Matuyama-Brunhes geomagnetic reversal in Chinese loess, *Geochem. Geophys. Geosyst.*, *15*, 4468–4480, doi:10.1002/2014GC005497.

Received 15 JUL 2014
Accepted 22 OCT 2014
Accepted article online 27 OCT 2014
Published online 28 NOV 2014

Apparent timing and duration of the Matuyama-Brunhes geomagnetic reversal in Chinese loess

Hui Zhao[1,2], Xiaoke Qiang[1], and Youbin Sun[1]

[1]State Key Laboratory of Loess and Quaternary Geology, Institute of Earth Environment, Chinese Academy of Sciences, Xian, China, [2]School of Resources and Environment, University of Chinese Academy of Sciences, Beijing, China

Abstract The Matuyama-Brunhes (MB) geomagnetic reversal in Chinese loess has been studied extensively as an important boundary for land-ocean stratigraphic and paleoclimatic correlations. However, the apparent timing and duration of the MB boundary remain controversial in Chinese loess deposits due to its inconsistent stratigraphic position and the uncertain chronologies. Here we synthesized high-resolution paleomagnetic records from four loess sequences in the central Chinese Loess Plateau and synchronized the loess-paleosol chronology by matching the grain-size variations to orbitally tuned grain-size time series. The synthesized paleomagnetic results reveal consistent features of the MB transition in Chinese loess, including the stratigraphic position (L_8/S_8 transition), timing (~808–826 ka), duration (~14–16 ka), and rapid directional oscillations. Compared with the MB transition in marine records (770–775 ka), the timing of the MB transition is relatively older and longer in Chinese loess, due to a complex interplay between different remanence acquisition mechanisms which occurred during the course of postdepositional physical and chemical processes.

1. Introduction

Chinese eolian deposit, covering an area of ~440,000 km^2 over the Chinese Loess Plateau (CLP), provides a unique terrestrial record of past climate and environmental changes since the late Oligocene [e.g., *Liu*, 1985; *Liu and Ding*, 1998; *An*, 2000; *Guo et al.*, 2002; *Qiang et al.*, 2011]. Changes in the geomagnetic field (i.e., polarity reversals and geomagnetic excursions) have been investigated extensively in Chinese loess and red clay sequences, and provide a reliable magnetostratigraphic framework for study of the East Asian monsoon evolution over the last 25 Ma [e.g., *Heller and Liu*, 1982; *Burbank and Li*, 1985; *Liu*, 1985; *Kukla*, 1987; *Liu et al.*, 1988; *Sun et al.*, 1998a; *Ding et al.*, 1999; *Guo et al.*, 2002; *Qiang et al.*, 2011]. In particular, the Matuyama-Brunhes (MB) geomagnetic reversal, as an important chronological marker for paleoclimatic correlation, has been studied extensively in Chinese loess deposits [e.g., *Heller and Liu*, 1982; *Sun et al.*, 1993; *Zhu et al.*, 1993, 1994, 1998; *Zhou and Shackleton*, 1999; *Spassov et al.*, 2001, 2003; *Wang et al.*, 2006; *Liu et al.*, 2008; *Yang et al.*, 2010; *Jin and Liu*, 2010, 2011a, 2011b; *Zhou et al.*, 2014; *Wang et al.*, 2014]. However, previous work suggested that the timing of the MB reversal in terrestrial loess is inconsistent with that in marine sediments, which has caused serious confusion in the stratigraphic correlation between loess and marine sequences [e.g., *Zhou and Shackleton*, 1999; *Wang et al.*, 2006; *Liu et al.*, 2008; *Jin and Liu*, 2011a; *Zhou et al.*, 2014].

In marine sediments, the MB reversal is generally located in marine oxygen isotope stage (MIS) 19 (an interglacial stage) [e.g., *deMenocal et al.*, 1990; *Tauxe et al.*, 1996; *Hyodo et al.*, 2006; *Liu et al.*, 2008; *Channell et al.*, 2004, 2009, 2010; *Suganuma et al.*, 2010, 2011], and its timing was recently constrained to be ~773.1 ± 0.4 ka [*Channell et al.*, 2010]. In Chinese loess, however, the stratigraphic position and timing of the MB reversal are spatially different, due to inconsistent criteria employed for stratigraphic division (Table 1, and references therein). For example, the MB transition occurred from the middle of L_8 to the top of S_8 at various loess sections, and the corresponding duration varies from 3.6 to 20 ka. Most paleomagnetic investigations suggested that the position of the MB reversal is likely located in lower part of L_8 (a glacial stage corresponding to MIS 20), in contrast to its counterpart in an interglacial stage (MIS 19) in the marine records. The inconsistency of the MB reversal in Chinese loess and marine sediments has been attributed to the complicated mechanism of remanent magnetization acquisition in loess that occurs at a certain depth substantially below the land surface [*Zhou and Shackleton*, 1999]. Detailed paleomagnetic investigation and redeposition

Table 1. Stratigraphic Position, Thickness, Timing and Duration of the MB Transition in Typical Loess Sections[a]

Section	Position	Thickness (cm)	Duration (kyr)	Stratigraphic Division[b]	Demagnetization Methods[b]	References	Timing (ka) in This Study
Luochuan	Lower L_8	50		MS	TD	*Zhu et al.* [1998]	
Luochuan	L_8/S_8 transition	40		MS and GS	TD	*Jin and Liu* [2010, 2011a]	820–825
Luochuan	Bottom L_8	70	15	MS	TD	*Zhou et al.* [2014]	810–825
Xifeng	Lower L_8	223	20	MS	TD	*Sun et al.* [1993]	
Xifeng	Lower L_8	36	3.6	MS	TD	*Zhu et al.* [1993]	
Xifeng	L_8/S_8 transitions	100	17.4	MS	TD and AFD	*Yang et al.* [2010]	810–826
Xifeng	Bottom L_8	100	16	MS	TD	*Zhou et al.* [2014]	810–826
Baoji	Lower L_8	70	10.3	MS	TD and AFD	*Yang et al.* [2010]	808–822
Baoji	Lower L_8	70		MS	TD	*Spassov et al.* [2001]	808–822
Lingtai	Middle L_8	50		MS	AFD	*Spassov et al.* [2001]	806–820
Weinan	Lower L_8	50	5	MS	TD	*Zhu et al.* [1994]	
Duanjiapo	Lower L_8	33		MS	TD	*Zhu et al.* [1998]	
Changwu	Lower L_8	40		MS	TD	*Zhu et al.* [1998]	
Yichuan	Lower L_8	50		MS	TD	*Zhu et al.* [1998]	
Sanmenxia	Top S_8	50	7.7	MS	TD	*Wang et al.* [2006]	
Mangshan	L_8/S_8 transition	85		MS and GS	TD	*Jin and Liu* [2011b]	

[a]The stratigraphic position was cited from the determination of the original references.
[b]Stratigraphic division criteria: MS, magnetic susceptibility and GS, grain size. Demagnetization methods: TD, thermal demagnetization and AFD, alternating-field demagnetization.

experiments reveal that the magnetization of Chinese loess appears to be controlled by a complex time-varying combination of depositional remanent magnetization (DRM), postdepositional remanent magnetization (PDRM), and chemical remanent magnetization (CRM) mechanisms [e.g., *Spassov et al*., 2003; *Zhao and Roberts*, 2010; *Wang and Løvlie*, 2010; *Wang et al*., 2006, 2014]. The interplay between different remanence acquisition mechanisms, particularly the PDRM and CRM, might cause variable downward displacement of the geomagnetic excursions and reversals in Chinese loess, which has been termed as a "lock-in effect" in previous paleomagnetic studies [e.g., *Zhou and Shackleton*, 1999; *Spassov et al*., 2003; *Zhu et al*., 2007; *Sun et al*., 2013].

The inconsistency of the timing of the MB reversal in terrestrial and marine records originated from the well accepted correlation between loess proxies and the marine oxygen isotope record, i.e., paleosol layers S_6 to S_8 were correlated to MIS 17 to 21 in previous land-ocean comparisons [e.g., *Liu*, 1985; *Kukla*, 1987; *Kukla and An*, 1989; *Ding et al*., 1995; *Bloemendal et al*., 1995; *Liu et al*., 1999; *Ding et al*., 2002]. Based on the assumption that the MB reversal is a global feature, this longstanding chronological conundrum for marine and Chinese loess sequences could potentially be solved by correlating S_8 to MIS 19 [e.g., *Wang et al*., 2006; *Liu et al*., 2008; *Jin and Liu*, 2011a]. Recently, the MB transition has been investigated using both paleomagnetic and cosmogenic ^{10}Be approaches [*Suganuma et al*., 2010, 2011; *Zhou et al*., 2014], suggesting that the effect of the geomagnetic signal through acquisition of the PDRM and CRM processes adds uncertainty to the synchronization of the MB transition in terrestrial and marine sedimentary records. To reevaluate the land-ocean inconsistency, it is critically important to make a close examination of the exact stratigraphic position, the apparent timing and duration, the detailed transitional features of the MB reversal in Chinese loess, and of the detailed land-ocean comparison based on two alternative age models (i.e., correlation of S_8 to MIS 19 and 21, respectively).

In this study, we first synthesized high-resolution paleomagnetic records of the MB transition at the Luochuan, Xifeng, Baoji, and Lingtai sections on the Chinese Loess Plateau after matching magnetic susceptibility (χ) and grain-size variations generated from different studies. The stratigraphic position of the MB reversal was redetermined based on grain-size variations. Similar to previous loess chronology and land-ocean correlations (i.e., matching S_8 to MIS 21), we then synchronized the grain-size variations of these four loess sections using an automatic orbital tuning approach to determine the apparent timing and duration of the MB reversal. In addition, an alternative age model was generated by correlating S_8 to MIS 19. The validity of the two different age models was evaluated by assessing the changes in sedimentation rates and making a detailed land-ocean comparison. Finally, the similarities and differences of the MB transition in Chinese loess and marine sediments may be linked with changes in relative geomagnetic paleointensity and pedogenic alteration. Unlike previous paleomagnetic work, which has attempted to elucidate the complex loess remanence acquisition mechanisms, here we address two basic issues related to the MB reversal

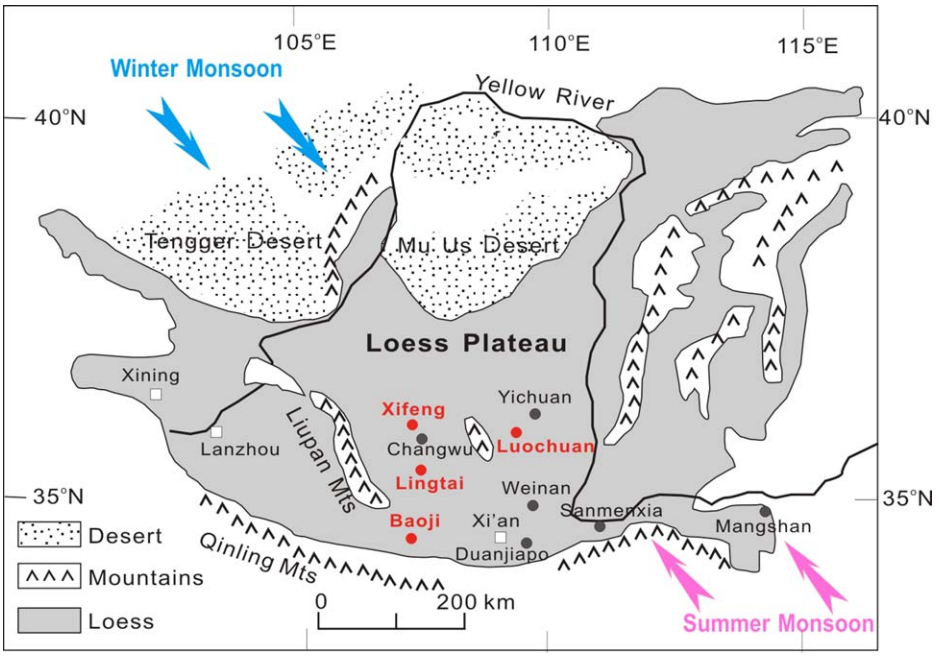

Figure 1. The Chinese Loess Plateau and location of the investigated loess sections. Red dots denote four loess sections with high-resolution paleomagnetic results discussed in this study.

in Chinese loess: the inconsistent stratigraphic position and poorly constrained timing of the MB reversal. Our objectives are to reconcile the stratigraphic position of the MB reversal in Chinese loess and to provide a better constraint of its apparent timing and duration.

2. High-Resolution Paleomagnetic Results From Four Loess Sequences

Paleomagnetic investigations have been conducted on many sections across the CLP (Figure 1). The MB reversal is characterized by rapid directional oscillations located between lower L_8 and upper S_8, with a transitional behavior at depths, varying from 33 to 223 cm (Table 1, and reference therein). For example, in the southeastern margin of the CLP, two loess sequences located at Sanmenxia and Mangshan were chosen for high-resolution paleomagnetic investigation of the MB reversal [*Wang et al*., 2006; *Jin and Liu*, 2011a]. The results suggest that the MB reversal is located at the L_8/S_8 boundary, whereas the thickness varied from 50 cm at Sanmenxia to 85 cm at Mangshan. In the central CLP, the stratigraphic position and thickness of the MB reversal vary across the nine sections (Table 1). Here we focus on four sections (Xifeng, Luochuan, Baoji, and Lingtai) where rapid directional oscillations during the MB reversal have been widely identified based on repeatable high-resolution paleomagnetic results. To facilitate the paleomagnetic comparison, we first standardize the depths of each section by matching the χ records from different studies. The latitude of the virtual geomagnetic pole (VGP) was then calculated using the published inclination and declination data of these sections (Figure 2). Since the MB reversal is characterized by several directional oscillations rather than an abrupt change, hereafter we use the term "MB transition" to reflect rapid VGP changes.

Reliable determination of the stratigraphic position of the MB transition needs a consistent criterion to define the loess-paleosol boundary. As pointed out by *Liu et al*. [2008], judgment of the stratigraphic boundary is not straightforward based on field observation or magnetic susceptibility variations. However, a similar pattern of grain-size variations across units S_7 and S_8 is observed at the four loess sections, enabling reliable stratigraphic correlations between the four sites (Figure 2). In contrast, χ variations exhibit different patterns between the northern (Luochuan and Xifeng) and southern (Lingtai and Baoji) sections, indicating that changes in local precipitation can cause significant variability in pedogenesis and associated magnetic susceptibility enhancement. Here we employed rapid changes in grain size for fine-scale interprofile correlations of the loess-paleosol boundaries. Below we summarize the main features of the MB transition based on the VGP data and rapid grain-size variations of the four loess sections.

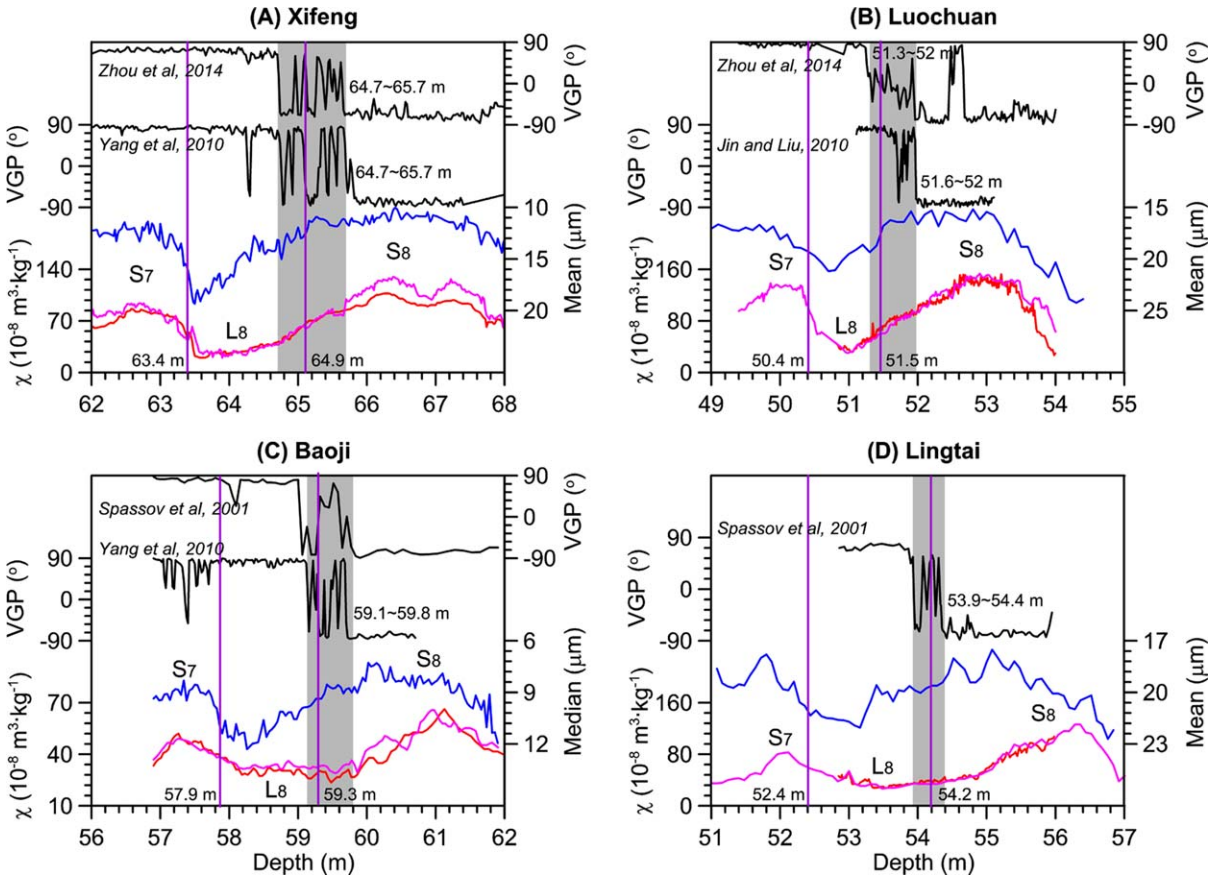

Figure 2. Magnetic susceptibility (χ, red and pink), grain size (blue), and latitude of the virtual geomagnetic pole (VGP, black) of four loess sections: (a) Xifeng [*Yang et al*., 2010; *Zhou et al*., 2014], (b) Luochuan [*Jin and Liu*, 2010; *Zhou et al*., 2014], (c) Baoji [*Spassov et al*., 2001; *Yang et al*., 2010], and (d) Lingtai [*Spassov et al*., 2001]. The depths for each section were unified by matching the χ records from different studies. Gray bars denote the MB transition inferred from the VGP latitudes. Thick purple lines indicate the loess/paleosol boundaries inferred from rapid grain-size variations. Note that the grain size proxies were derived from bulk samples for BJ and LC sections [*Ding et al*., 2002], and from quartz particles for LT and XF sections [*Sun et al*., 2006a].

The Xifeng (XF) section (35.7°N, 107.6°E) is situated in the largest tableland (namely Dongzhi Yuan) in the central CLP (Figure 1), where the mean annual precipitation (MAP) is about 550 mm. The Quaternary loess-paleosol sequence in this region is about 170 m in thickness, and is underlain by ~60 m of Neogene red-clay deposits [*Sun et al*., 1998b]. As a typical loess section, many researchers have conducted paleomagnetic work on the loess sequences developed in this region [e.g., *Liu et al*., 1988; *Sun et al*., 1993; *Zhu et al*., 1993, *Yang et al*., 2010; *Zhou et al*., 2014]. Earlier work demonstrated that the MB boundary is located in the lower part of loess unit L_8 [*Liu et al*., 1988; *Sun et al*., 1993; *Zhu et al*., 1993, 1998]. However, the thickness of the MB transition is quite variable, from 36 to 223 cm [*Sun et al*., 1993; *Zhu et al*., 1993]. Recently, the results of a high-resolution paleomagnetic investigation using both thermal demagnetization (TD) and alternating-field demagnetization (AFD) treatments suggested that the MB transition is located around the L_8/S_8 transition (Figure 2a), spanning an interval of ca. 100 cm [*Yang et al*., 2010; *Zhou et al*., 2014].

The Luochuan (LC) section (35.7°N, 109.4°E) is located in the central CLP (Figure 1), where the MAP is about 610 mm. This section has been studied as a classic loess section for half a century [e.g., *Liu*, 1966; *Heller and Liu*, 1982; *Liu*, 1985; *An et al*., 1990; *Xiao and An*, 1999; *Lu et al*., 1999]. The total thickness of the Quaternary loess-paleosol sequence is about 135 m, and is underlain by ~15 m of Pliocene red-clay deposits [*Liu*, 1985]. The magnetostratigraphy of the LC section has been investigated by many researchers [e.g., *Heller and Liu*, 1982; *Kukla and An*, 1989; *Zhu et al*., 1998; *Liu et al*., 2010; *Zhou et al*., 2014]. Earlier low-resolution paleomagnetic results revealed an abrupt reversal ranging from the top of S_8 to L_8 [e.g., *Heller and Liu*, 1982; *Liu*, 1985; *Zhu et al*., 1993]. *Zhu et al*. [1998] first collected continuous oriented samples from L_8 to S_8 for TD measurements, and observed a distinct polarity transition zone in the lower part of L_8, with an interval of ca. 50 cm.

Recently, *Jin and Liu* [2010] also investigated the MB transition using 10 parallel subsamples collected at a ~2 cm resolution from the outcrop. The paleomagnetic results also revealed a distinct polarity transition zone corresponding to low relative paleointensity (RPI) at the L_8/S_8 boundary, with an interval of ca. 40 cm (Figure 2b). A similar high-resolution magnetostratigraphic investigation by *Zhou et al*. [2014] confirmed that the MB transition was located around the L_8/S_8 boundary, with an interval of directional oscillations of ca. 70 cm (Figure 2b).

The Baoji (BJ) section (34.41°N, 107.12°E) is in the southern part of the CLP (Figure 1), where the MAP is around 660 mm. The Quaternary loess-paleosol sequence in this section is around 160 m in thickness, with 37 pedostratigraphic units (S_0 to L_{33}) clearly identified from the field outcrops [*Rutter et al*., 1990, 1991; *Ding et al*., 1993]. Early paleomagnetic results showed that the MB boundary is located within loess unit L_8 [*Rutter et al*., 1990; *Yang et al*., 2004]. Based on high-resolution TD results, *Spassov et al*. [2001] found that the MB transition at the BJ section is characterized by five directional changes over a transitional interval of ca. 70 cm within the lower part of L_8 (Figure 2c). A similar stratigraphic location and rapid swings were confirmed by a subsequent high-resolution paleomagnetic investigation of the BJ section [*Yang et al*., 2010].

The Lingtai (LT) section (34.9°N, 107.5°E, 1340 m a.s.l.) is located between the XF and BJ profiles (Figure 1), where the MAP is 650 mm. The field outcrops at the LT section consist of two parts: the upper loess-palaeosol sequence with a thickness of 166 m and the lower 120 m red-clay formation [*Sun et al*., 1998a; *Ding et al*., 1999]. Early low-resolution magnetostratigraphic studies demonstrated that the MB boundary is located in the lower part of L_8 [*Sun et al*., 1998a; *Ding et al*., 1999]. Subsequent high-resolution paleomagnetic results demonstrated that seven directional changes occurred within a transitional interval of ca. 50 cm in the middle part of L_8 (Figure 2d) [*Spassov et al*., 2001].

3. Synchronization of the Loess-Paleosol Chronology

The loess-paleosol chronologies have been generated using a magnetic susceptibility model [*Kukla et al*., 1988], a grain-size model [*Porter and An*, 1995; *Vandenberghe et al*., 1997], and an orbital tuning approach [*Ding et al*., 1994, *Lu et al*., 1999; *Heslop et al*., 2000; *Ding et al*., 2002; *Sun et al*., 2006a, 2006b]. Although the rationale of the various age models is different, the resulting time series of magnetic susceptibility and grain size are well correlated with the marine oxygen isotope record [*Kukla and An*, 1989; *Ding et al*., 1995; *Bloemendal et al*., 1995; *Liu et al*., 1999; *Ding et al*., 2002]. Especially for the last 900 ka, the nine loess-paleosol alternations (S_0 to L_9) correspond well with MIS 1 to 24 suggesting a strong coupling between the East Asian monsoon and changes in northern hemisphere ice volume [*Ding et al*., 1995; *Hao et al*., 2012].

Since grain size records spanning the entire loess-paleosol sequences were available for four loess sections (i.e., Xifeng, Luochuan, Lingtai, and Baoji), we focus on these four sections for further chronological synchronization and intersection comparison. The chronologies of these four sections have been reconstructed using orbital tuning methods [*Lu et al*., 1999; *Heslop et al*., 2000; *Ding et al*., 2002; *Sun et al*., 2006a]. However, there are subtle inconsistencies among these age models due to the different tuning proxies and target curves used (see a detailed comparison in *Sun et al*. [2006a]). In order to eliminate any chronological uncertainties, we synchronized the grain-size variations of the Luochuan and Baoji sections to previously published grain-size time series of the Xifeng and Lingtai sections by matching S_8 to MIS 21 [*Sun et al*., 2006a]. Although the grain size proxies generated from bulk and quartz samples are slightly different [*Sun et al*., 2006c], these proxies from four loess sections display similar variations at glacial-interglacial timescales (Figure 2). Thus, different grain size proxies were normalized (hereafter referred to as normalized grain size, NGS) for further orbital tuning and intersection correlation.

The chronologies for the Baoji and Luochuan sections were refined using the automatic orbital tuning method proposed by *Yu and Ding* [1998], which has been employed successfully in the astronomical calibration of the loess chronologies [e.g., *Ding et al*., 2001, 2002; *Sun et al*., 2006a, 2006b]. The tuning method involves four steps as follows: (1) selection of the tuning targets, (2) construction of an initial timescale, (3) orbital tuning of the initial timescale, and (4) finely tuning the age of each depth. The tuning targets were generated from the orbital solution of *Berger* [1978], employing the SPECMAP-defined lag of 5 and 8 kyr for obliquity and precession [*Imbrie et al*., 1984], respectively. Based on the previous astronomical timescales [*Lu et al*., 1999; *Heslop et al*., 2000; *Ding et al*., 2002; *Sun et al*., 2006a], we selected the ages of the loess-paleosol boundaries as tie points to generate an initial timescale for orbital tuning. The ages of these time

controls were adjusted to achieve a high correlation of the filtered 41 and 23 kyr components of the NGS to the lagged obliquity and precession parameters. Finally, the age of each depth was finely tuned using a dynamical optimization method.

The validity of the age model (here after referred as AM1) was evaluated using three independent approaches. First, based upon the synchronized chronologies, grain-size variations of these four sections are highly consistent with each other (Figure 2), including the glacial-interglacial cycles and the precessional-scale oscillations in thick loess layers (e.g., L_2, L_5, L_6, and L_9). The NGS time series are also high correlated with the stacked quartz grain size (QGS) record, with coefficients ($n = 951$) of 0.7 at BJ, 0.71 at LC, 0.89 at LT, and 0.93 at XF. The rather low coefficients at BJ and LC may be attributable to the fact that the grain size results were obtained on bulk samples. Second, the NGS variations were compared with the marine oxygen isotope record [*Lisiecki and Raymo*, 2005] and northern hemisphere July insolation [*Berger*, 1978]. Consistent with previous land-ocean comparisons [*Liu*, 1985; *Kukla*, 1987; *Bloemendal et al*., 1995; *Ding et al*., 1995, 2002; *Liu et al*., 1999], the most developed paleosol complex S_5 is correlated to MIS 13 to 15, and S_6 to S_8 are corresponded to MIS 17 to 21, respectively (Figure 3). Note that four NGS time series show two evident peaks in four weakly weathered loess layers of L_2, L_5, L_6, and L_9. These peaks correspond well to similar precessional-scale insolation maxima (Figure 3), but are not evident in the benthic δ^{18}O record, due to the 180° out-of-phase nature of southern-hemisphere and northern-hemisphere heating/cooling in the precessional band [*Clemens*, 1999]. Third, comparison of the filtered components of the NGS with the lagged obliquity and precession curves suggests that our tuned timescales are well constrained by the obliquity and precession parameters (Figure 4). Generally, the filtered 41 and 21 kyr components of the four NGS records are in phase with the lagged obliquity and precession curves, with correlation coefficients ranging between 0.73 and 0.84 in the obliquity band and between 0.65 and 0.78 in the precession band, respectively.

We are aware that there is an alternative way to explain the age of the MB boundary in Chinese loess. As suggested by several studies [*Wang et al*., 2006; *Liu et al*., 2008; *Jin and Liu*, 2010, 2011a], the MB position at the L_8/S_8 boundary is consistent with its counterpart in marine sediments by assuming that S_8 is correlated to MIS 19. Following this land-ocean comparison strategy, an alternative age model (hereafter referred to as AM2) was generated by matching the MBB at ~770 ka for the Luochuan section and expanding L_9 to 790–930 ka, as proposed by *Liu et al*. [2008] and *Jin and Liu* [2011a, 2011b]. We only select the Luochuan section because it has been studied as a classic loess sequence for many decades, and displays proxy variations similar to the other three sections (Figure 3).

Compared to AM1, paleosols S_6 to S_8 in AM2 were compressed to 680–790 ka and corresponded to MIS 17 to 19, whereas the thick loess unit (L_9) was expanded to 790–930 ka and correlated to MIS 20 to 24 (Figure 5). We evaluated the reliability of these two age models using two approaches. First, we made a peak-by-peak correlation of loess grain size (LC NGS) and magnetic susceptibility (χ) with the benthic δ^{18}O stack, with special attention paid to the amplitude match between these proxies during MIS 17 to 24. The δ^{18}O amplitude in MIS 21 is comparable to that in MIS 17 and 19, whereas in AM2 the grain size and χ are significantly lower in upper L_9 (MIS 21) compared to that of S_6 to S_8 (MIS 17 and 19). In AM1, however, the amplitude of two loess proxies from S_6 to S_7 and marine δ^{18}O during MIS 17 to 21 are comparable. Therefore, correlation of L_9 (a thick, silty loess layer) to MIS 20 to 24 in AM2 seems unreasonable because of the amplitude mismatch between loess proxies and benthic δ^{18}O in MIS 21.

Second, sedimentation rate (SR) change is another criterion for evaluating the validity of the loess chronology. It is well accepted that the SR in interglacial paleosols is lower than in glacial loess layers, due to the shrinkage of the dust source areas and the weakening of the winter monsoon during warm and humid interglacials [*Liu et al*., 1985; *An et al*., 1991; *Ding et al*., 2005]. *Ding et al*. [2001] further suggested coeval changes between grain size and sedimentation rate of Chinese loess at glacial-interglacial timescales. The SR fluctuations of the Luochuan section in AM1 exhibit distinct glacial-interglacial variations, with low SR in paleosols and high SR in loess layers (Figure 5). Specifically in L_9, the SR (8–20 cm/kyr) is higher than that of overlying paleosol and loess layers (S_6 to S_8, ~5 cm/kyr), because L_9 is a thick silty layer related to desert expansion and global cooling [*Sun and Liu*, 2000; *Ding et al*., 2005]. In AM2, however, the SR (8.3 cm/kyr) in upper L_9 is comparable to that of overlying S_8. Notably, the SR in lower L_9 is significantly low (3 cm/kyr) due to its expansion to MIS 22 to 24. The SR change based upon AM2 is inconsistent with the generally accepted accumulation model of Chinese loess, implying that AM2 is unreasonable. Therefore, we adopted AM1 as a well-accepted chronology to further address the timing of the MB transition in Chinese loess. Nevertheless,

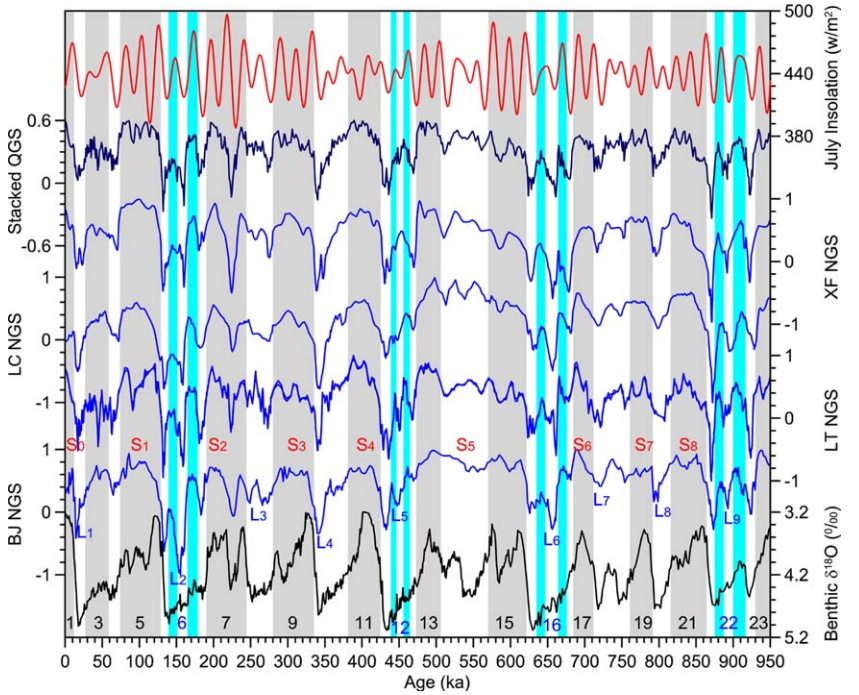

Figure 3. Comparison of the normalized grain size (NGS, blue) variations of four loess sections with stacked quartz grain size (QGS, dark blue) record [*Sun et al*., 2006a], northern hemisphere July insolation (red) [*Berger*, 1978], and the benthic $\delta^{18}O$ record (black) [*Lisiecki and Raymo*, 2005]. Gray bars indicate the correlation between paleosol layers (S_0 to S_9) and interglacial marine isotope stages (MIS 1 to 21). Sky blue bars indicate that the grain size peaks in four thick loess layers (L_2, L_5, L_6, L_9) correspond to precessional insolation maxima.

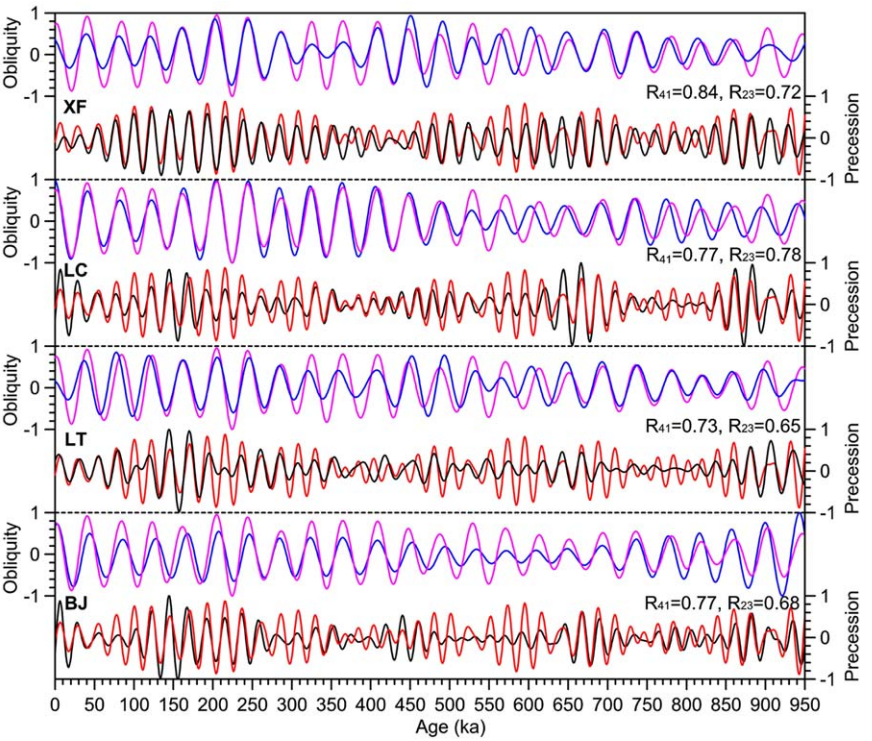

Figure 4. Four NGS time series filtered at 41 kyr (blue) and 23 kyr (black) bands and their comparison with lagged obliquity (pink) and precession (red). Both the filtered signals and orbital records are normalized. R_{41} and R_{23} denote the correlation coefficients between the filtered components and orbital parameters.

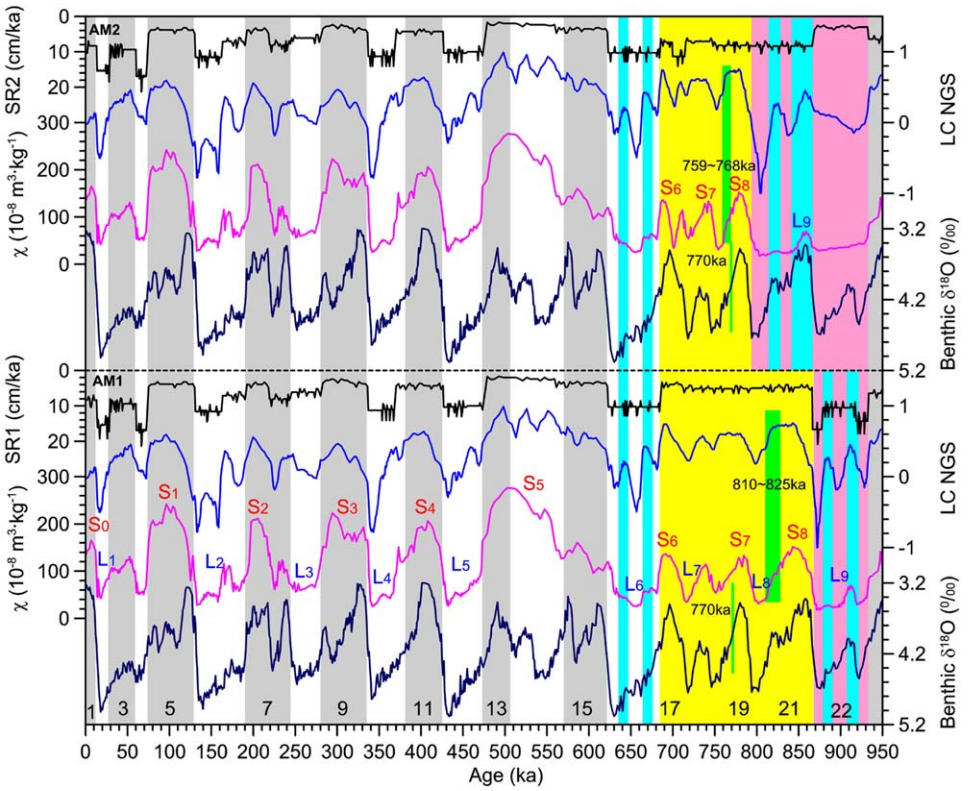

Figure 5. Comparison of χ, NGS, and sedimentation rate (SR) of the Luochuan sections (based on two different age models) with the benthic $\delta^{18}O$ record [*Lisiecki and Raymo*, 2005]. The major difference between AM1 and AM2 lies in the correlation between S_6 to L_9 and MIS 17 **to** 24. The yellow box indicates that S_6 to S_8 were compressed in AM2 compared to AM1, while the pink box indicates that the L_9 was expanded in the AM2 relative to the AM1. Blue sky bars indicate that two grain size peaks in L_6 are identical in both age models, whereas the grain size peaks in L_9 were shifted to significantly younger ages in AM2 relative to AM1. Green bars denote the MB transition with different ages in these two age models.

since these two models were generated on the basis of different matching strategies between loess grain size and marine $\delta^{18}O$ records, absolute dating of the S_8 in the future would permit more reliable land-ocean correlations.

4. Timing, Duration, and Rapid Swings of the MB Transition in Chinese Loess

Based on the synchronized age models and grain-size variations, the ages of the S_8/L_8 and L_8/S_7 boundaries are determined as 814 and 792 ka, respectively, and the stratigraphic positions of the MB transition for each site are all located in the S_8/L_8 transitional zone (Figure 6). The timing of the MB transition at the XF section is almost identical (810–826 ka) in two parallel paleomagnetic investigations [*Yang et al*., 2010; *Zhou et al*., 2014]. For the LC section, the termination of the MB transition is significantly older in the paleomagnetic results of *Jin and Liu* [2010] than in those of *Zhou et al*. [2014], although the timing of the onset of the MB transition is almost identical in these two studies. The timing of the MB transition at BJ is almost identical in two paleomagnetic studies (808–822 ka) [*Spassov et al*., 2001; *Yang et al*., 2010]. For the LT section, the MB transition occurred during the interval of 806–820 ka [*Spassov et al*., 2001]. In summary, the onset of the timing of the MB transition varies from 820 to 826 ka, while its terminal age ranges from 806 to 810 ka, except in the LC paleomagnetic results of *Jin and Liu* [2010]. Consequently, the duration of the MB transition can be estimated as ranging from 14 to 16 kyr in these four loess sections.

It is noteworthy that the timing of the MB transition is slightly younger (~2–4 ka) at LT and BJ than that at XF and LC, possibly due to the differences in MAP and lithology. Since the MAP of LT and BJ (650–660 mm) is higher than that of XF and LC (550–610 mm), they may have undergone strong pedogenesis resulting in relatively high clay content. The grain size at LT and BJ is clearly finer than that at XF and LC, because of the relatively strong pedogenesis and the long distance to the potential dust sources [*Hao and Guo*, 2005; *Yang*

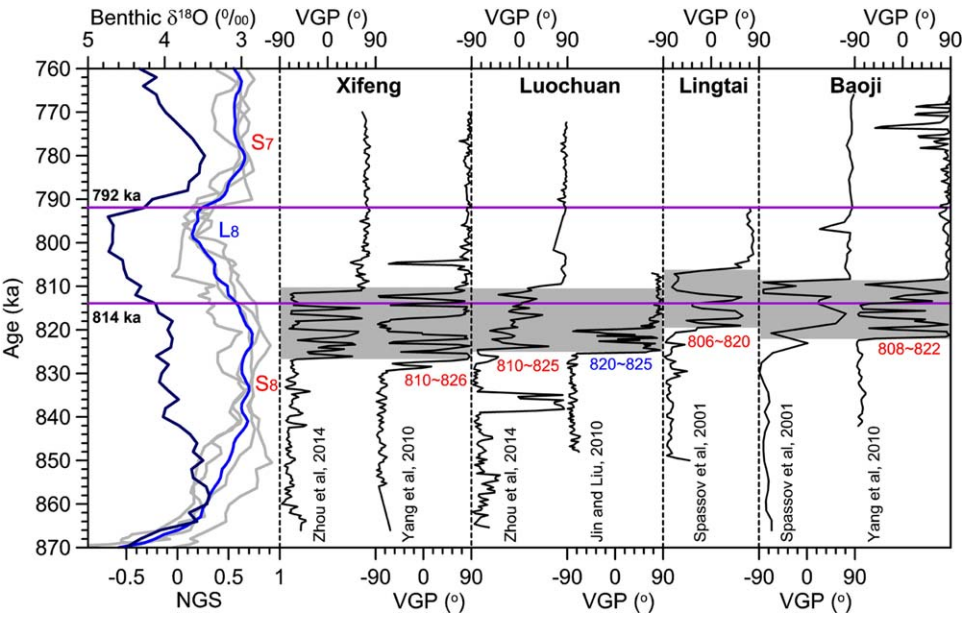

Figure 6. VGP records (black) of four loess sections and their comparison with the benthic $\delta^{18}O$ record (dark blue) [*Lisiecki and Raymo*, 2005] and the stacked NGS record (blue) of four sections. The original NGS data of the four sections are shown as light gray curves. Gray bars denote the MB transition. Purple lines indicate the loess/paleosol boundaries.

and Ding, 2008]. Comparison of the MB boundary in Eurasian loess deposits revealed that if a loess sequence contains relatively high clay content, a suitable microenvironment for remanence acquisition may be formed at a relatively shallow depth [*Zhou and Shackleton*, 1999]. Recently, laboratory experiments suggest that water content plays the most important control in the PDRM acquisition of loess [*Zhao and Roberts*, 2010; *Wang and Løvlie*, 2010]. The depth of precipitation infiltration is likely to decrease in soils with increasing clay content [*Helalia*, 1993]. In addition, a recent study indicated that relatively high clay content generally resulted in low saturated hydraulic conductivity values [*Wang et al*., 2013]. A shallow water-saturated zone can also cause a limited downward displacement of the MB boundary relative to the initial position. Therefore, the lock-in depth of the PDRM process in Chinese loess may be influenced by multiple factors, such as surface mixing, pedogenesis, lithology, and leaching intensity [e.g., *Sun et al*., 1993; *Zhu et al*., 1994, 1998; *Liu et al*., 2008; *Sun et al*., 2013]. All of these factors could potentially result in subtle differences in the timing and duration of the MB transition in various loess sections.

Another notable feature of the MB transition is the rapid directional oscillations; however, the exact number of the swings differs from site to site, e.g., 12 swings at XF and LC [*Zhou et al*., 2014], and six swings at LT and BJ [*Spassov et al*., 2001] (Figure 6). Similar rapid directional swings during the MB transition were also identified at Weinan, Duanjiapo, Yichuan, Changwu, Sanmenxia, and Mangshan (Table 1, and references therein), and extended to the upper Jaramillo/Matuyama and Gauss/Matuyama boundaries [*Zhu et al*., 1994; *Yang et al*., 2014]. A theoretical model reveals that the same geomagnetic polarity transition should be repeatable in various locations [*Jacobs*, 1994; *Meeril et al*., 1996]. Two possible mechanisms have been proposed to interpret these directional oscillations. One is that the weak geomagnetic field was not strong enough efficiently to realign the detrital magnetite grains, resulting in a disorderly distribution of paleomagnetic directions [*Zhou and Shackleton*, 1999; *Jin and Liu*, 2010]. Another possibility is that the MB transitional zone was formed by overprinting of the PDRM and/or CRM processes, which could have disturbed the original directions by varying degrees [*Guo et al*., 2001; *Spassov et al*., 2003; *Wang et al*., 2014]. Hence, the mechanisms responsible for the rapid directional swings during polarity reversal merit further investigation, especially using parallel paleomagnetic and ^{10}Be records [*Suganuma et al*., 2010, 2011; *Zhou et al*., 2014].

5. Comparison of the MB Transition in Chinese Loess and Marine Sediments

High-resolution paleomagnetic results from Chinese loess have been compared with the VGP and relative paleointensity records documented in marine sediments [e.g., *Liu et al*., 2008; *Zhou et al*., 2014]. Similar to

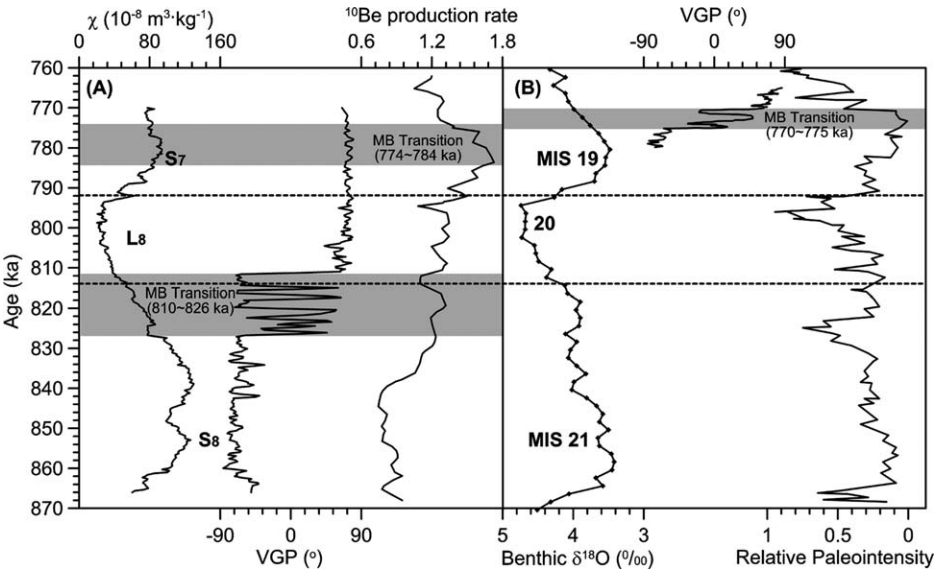

Figure 7. Comparison of (a) χ, VGP latitude, and ^{10}Be production rate (normalized) of the Luochuan section [*Zhou et al*., 2014] with (b) benthic δ^{18}O, VGP latitude, and relative paleointensity (RPI) records of ODP Site 983 [*Channell and Kleiven*, 2000]. Gray bars denote the MB transition inferred from the VGP, ^{10}Be production rate, and relative paleointensity records. Dashed lines indicate the correlation of the S_7/L_8 and L_8/S_8 boundaries to MIS 19/20 and 20/21, respectively.

the MB transition in Chinese loess, the MB transition in deep-sea sediments is also characterized by rapid directional changes (Figure 6), as seen in the VGP records of ODP Sites 983 and 1063 from the North Atlantic [*Channell and Kleiven*, 2000; *Channell et al*., 2010]. This feature is especially clear in cores with high sediment accumulation rates (10 cm/kyr or more) [e.g., *Okada and Niitsuma*, 1989; *Yamazaki and Oda*, 2001; *Channell et al*., 2004; *Hyodo et al*., 2006]. It is noteworthy that the lock-in depth for the MB transition is fairly shallow in marine sediments [e.g., *Tauxe et al*., 1996; *Bleil and von Dobeneck*, 1999; *Horng et al*., 2002]. A recent paleomagnetic study of three piston cores from the western Pacific Ocean indicated a ~15 cm downward offset of the paleointensity minimum relative to the ^{10}Be flux anomaly [*Suganuma et al*., 2010], indicating a shallower PDRM lock-in depth in marine sediment than in loess [e.g., *Zhou and Shackleton*, 1999; *Spassov et al*., 2003; *Zhou et al*., 2014]. Moreover, the record of higher-frequency geomagnetic field changes in marine sediment may be smoothed by a slow accumulation rate and the filtering effect of the PDRM process [*Hyodo*, 1984]. Nevertheless, rapid directional changes in marine sediment may mainly reflect the behavior of the geomagnetic field [e.g., *Oda et al*., 2000; *Yamazaki and Oda*, 2001; *Channell et al*., 2004]; for example, the results of *Hyodo et al*. [2006] are compatible with numerical simulations of a geomagnetic field reversal [*Glatzmaier and Roberts*, 1995].

Our results confirm that the MB transition is located around the MIS 21/20 boundary in Chinese loess, consistent with early land-ocean comparisons of the MB boundary [*Tauxe et al*., 1996; *Zhou and Shackleton*, 1999, and references therein]. In marine sediments, however, the MB boundary most likely occurs in late MIS 19 (an interglacial stage) [e.g., *Liu et al*., 2008; *Tauxe et al*., 1996; *Channell et al*., 2010, and references therein]. By synchronizing the timing of the MB boundary in Chinese loess and marine records, several studies have argued that paleosol unit S_8 should correspond to MIS 19 instead of MIS 21 [e.g. *Liu et al*., 2008; *Yang et al*., 2010; *Wang et al*., 2006; *Jin and Liu*, 2011a]. This adjustment may bring the marine and terrestrial records into better age agreement for the MB boundary, but would result in a confused cycle-to-cycle correlation of Chinese loess-paleosol sequences to the marine isotope stages.

We also compare the loess-derived VGP and ^{10}Be production rate records of the Luochuan section [*Zhou et al*., 2014] with the VGP and RPI records of ODP Site 983 [*Channell and Kleiven*, 2000] (Figure 7). In marine sediments, the MB transition is correlated with low RPI values. However, our synthesized results indicate that the MB transition occurs during the time interval of 810–826 ka, indicating a large downward offset compared to the MB transition in marine sediment. However, reproducible ^{10}Be records of geomagnetic field intensity from the LC and XF loess sections exhibit a maximum production rate in S_7 (774–784 ka), slightly older than the timing of the MB reversal in the marine record (770–775 ka). The parallel ^{10}Be and

paleomagnetic records suggest that the classical loess-ocean correlations seem reasonable, e.g., S_7 and S_8 corresponding to MIS 19 and 21, respectively. Moreover, rapidly directional oscillations during the MB transition have been widely identified in loess sections and marine sediment cores, confirming the rapidly changing character of the MB transition in terrestrial and marine sediments. However, the magnitude and duration of these swings are variable from land to ocean. Such a land-ocean discrepancy is likely attributable to complex postdepositional physical and chemical processes, together with a variable sedimentary environment (e.g., changes in sedimentation rate, surface mixing, and different lithologies), which can lead to an inconsistent appearance of the spurious polarity swings.

6. Conclusions

A synthesis of high-resolution paleomagnetic records from four loess sequences (Xifeng, Luochuan, Baoji, and Lingtai) in the central Chinese Loess Plateau indicates that the MB geomagnetic reversal can be identified consistently in the L_8/S_8 transition and is characterized by rapid directional oscillations. After synchronizing the loess-paleosol chronologies to previously published orbital age models, the timing of the MB transition is estimated to be ca. 808–826 ka with durations ranging from 14 to 16 kyr. Our results reveal approximately consistent timing, duration, and transitional feature of the MB geomagnetic reversal in Chinese loess. Compared with the MB reversal in marine records (770–775 ka), the timing and duration of the MB transition are relatively old and long in Chinese loess, due to the complexity of remanence acquisition processes in terrestrial and marine sediments. In particular, a complex interplay between different remanence acquisition mechanisms, which occurred during the postdepositional physical and chemical processes, played an important role in resulting in a downward displacement (lock-in effect) of the MB transition in Chinese loess relative to deep-sea sediments.

Acknowledgments

We thank Jan Bloemendal, Andrew Roberts, Qingsong Liu, and three anonymous reviewers for valuable suggestions. This work was supported by grants from the Ministry of Science and Technology of China (2013CB955900), the Chinese Academy of Sciences (XDB03020504 and KZZD-EW-TZ-03), and the Natural Science Foundation of China (41272208). The data for this paper will be available for free at NOAA's Paleoclimatology data center.

References

An, Z. S. (2000), The history and variability of the East Asian paleomonsoon climate, *Quat. Sci. Rev.*, *19*, 171–187.

An, Z. S., T. S. Liu, Y. C. Lu, S. C. Porter, G. Kukla, X. H. Wu, and Y. M. Hua (1990), The long-term palaeomonsoon variation recorded by the loess-palaeosol sequence in central China, *Quat. Int.*, *7/8*, 91–95.

An, Z. S., G. Kukla, S. C. Porter, and J. L. Xiao (1991), Late quaternary dust flow on the Chinese Loess Plateau, *Catena*, *18*(2), 125–132.

Berger, A. (1978), Long-term variations of caloric insolation resulting from the Earth's orbital elements, *Quat. Res.*, *9*, 139–167.

Bleil, U., and T. von Dobeneck (1999), Geomagnetic events and relative paleointensity records—Clues to high-resolution paleomagnetic chronostratigraphies of Late Quaternary marine sediment?, in *Use of Proxies in Paleoceanography: Examples From the South Atlantic*, edited by G. Fischer and G. Wefer, pp. 635–654, Springer, Berlin.

Bloemendal, J., X. M. Liu, and T. C. Rolph (1995), Correlation of the magnetic susceptibility stratigraphy of Chinese loess and the marine oxygen isotope record, chronological and palaeoclimatic implications, *Earth Planet. Sci. Lett.*, *131*, 371–380.

Burbank, D. W., and J. J. Li (1985), Age and palaeoclimatic significance of the loess of Lanzhou, north China, *Nature*, *316*, 429–431.

Channell, J. E. T., and H. F. Kleiven (2000), Geomagnetic palaeointensities and astrochronological ages for the Matuyama Brunhes boundary and the boundaries of the Jaramillo Subchron: Palaeomagnetic and oxygen isotope records from ODP Site 983, *Philos. Trans. R. Soc. London A*, *358*, 1027–1047, doi:10.1098/rsta.2000.0572.

Channell, J. E. T., J. H. Curtis, and B. P. Flower (2004), The Matuyama-Brunhes boundary interval (500–900 ka) in North Atlantic drift sediments, *Geophys. J. Int.*, *158*, 489–505.

Channell, J. E. T., C. Xuan, and D. A. Hodell (2009), Stacking paleointensity and oxygen isotope data for the last 1.5 Myrs (PISO-1500), *Earth Planet. Sci. Lett.*, *283*, 14–23.

Channell, J. E. T., D. A. Hodell, B. S. Singer, and C. Xuan (2010), Reconciling astrochronological and $^{40}Ar/^{39}Ar$ ages for the Matuyama-Brunhes boundary and late Matuyama Chron, *Geochem. Geophys. Geosyst.*, *11*, Q0AA12, doi:10.1029/2010GC003203.

Clemens, S. C. (1999), An astronomical tuning strategy for Plio-Pleistocene sections: Implications for global-scale correlation and phase relationships, *Philos. Trans. R. Soc. London A*, *357*, 1949–1974.

deMenocal, P. B., W. F. Ruddiman, and D. V. Kent (1990), Depth of post-depositional remanence acquisition in deep-sea sediments: A case study of the Brunhes-Matuyama reversal and oxygen isotopic Stage 19.1, *Earth Planet. Sci. Lett.*, *99*, 1–13.

Ding, Z. L., N. W. Rutter, and T. S. Liu (1993), Pedostratigraphy of China loess deposits and climatic cycle in the last 2.5 Myr, *Catena*, *20*, 73–91.

Ding, Z. L., Z. W. Yu, N. W. Rutter, and T. S. Liu (1994), Towards an orbital time scale for Chinese loess deposits, *Quat. Sci. Rev.*, *13*, 39–70.

Ding, Z. L., T. S. Liu, R. W. Rutter, Z. W. Yu, Z. T. Guo, and R. X. Zhu (1995), Ice-volume forcing of East Asian winter monsoon variations in the past 800,000 years, *Quat. Res.*, *44*, 149–159.

Ding, Z. L., S. F. Xiong, J. M. Sun, S. L. Yang, Z. Y. Gu, and T. S. Liu (1999), Pedostratigraphy and paleomagnetism of a ~7.0 Ma eolian loess red clay sequences at Lingtai, Loess Plateau, north-central China and implications for paleomonsoon evolution, *Palaeogeogr. Palaeoclimatol. Palaeoecol.*, *152*, 49–66.

Ding, Z. L., Z. W. Yu, S. L. Yang. J. M. Sun, S. F. Xiong, and T. S. Liu (2001), Coeval changes in grain size and sedimentation rate of eolian loess, the Chinese Loess Plateau, *Geophys. Res. Lett.*, *28*, 2097–2100.

Ding, Z. L., E. Derbyshire, S. L. Yang, Z. W. Yu, S. F. Xiong, and T. S. Liu (2002), Stacked 2.6-Ma grain size record from the Chinese loess based on five sections and correlation with the deep-sea $\delta^{18}O$ record, *Paleoceanography*, *17*(3), doi:10.1029/2001PA000725.

Ding, Z. L., E. Derbyshire, S. L. Yang, J. M. Sun, and T. S. Liu (2005), Stepwise expansion of desert environment across northern China in the past 3.5 Ma and implications for monsoon evolution, *Earth Planet. Sci. Lett.*, *237*, 45–55.

Glatzmaier, G. A., and P. H. Roberts (1995), A three-dimensional self-consistent computer simulation of a geomagnetic field reversal, *Nature*, *377*, 203–209.
Guo, B., R. X. Zhu, F. Florindo, Y. X. Pan, and L. P. Yue (2001), Pedogenesis affecting the Matuyama-Brunhes polarity transition recorded in Chinese loess, *Chin. Sci. Bull.*, *46*(12), 975–981.
Guo, Z. T., W. F. Ruddiman, Q. Z. Hao, H. B. Wu, Y. S. Qiao, R. X. Zhu, S. Z. Peng, J. J. Wei, B. Y. Yuan, and T. S. Liu (2002), Onset of Asian desertification by 22 Myr ago inferred from loess deposit in China, *Nature*, *416*, 159–163.
Hao, Q. Z., and Z. T. Guo (2005), Spatial variations of magnetic susceptibility of Chinese loess for the last 600 kyr: Implications for monsoon evolution, *J. Geophys. Res.*, *110*, B12101, doi:10.1029/2005JB003765.
Hao, Q. Z., et al. (2012), Delayed build-up of Arctic ice sheets during 400,000-year minima in insolation variability, *Nature*, *490*(7420), 393–396.
Helalia, A. M. (1993), The relation between soil infiltration and effective porosity in different soils, *Agric. Water Manage.*, *24*, 39–47.
Heller, F., and T. S. Liu (1982), Magnetostratigraphical dating of loess deposits in China, *Nature*, *300*(5891), 431–433.
Heslop, D., C. G. Langereis, and M. J. Dekkers (2000), A new astronomical timescale for the loess deposits of northern China, *Earth Planet. Sci. Lett.*, *184*, 125–139.
Horng, C. S., M. Y. Lee, H. Palike, K. Y. Wei, W. T. Liang, Y. Iizuka, and M. Torii (2002), Astronomically calibrated ages for geomagnetic reversals within the Matuyama chron, *Earth Planets Space*, *54*, 679–690.
Hyodo, M. (1984), Possibility of reconstruction of the past geomagnetic field from homogeneous sediments, *J. Geomagn. Geoelectr.*, *36*, 45–62.
Hyodo, M., D. K. Biswas, T. Noda, N. Tomioka, T. Mishima, C. Itota, and H. Sato (2006), Millennial- to submillennial-scale features of the Matuyama-Brunhes geomagnetic polarity transition from Osaka Bay, southwestern Japan, *J. Geophys. Res.*, *111*, B02103, doi:10.1029/2004JB003584.
Imbrie, J., J. D. Hays, D. B. Martinson, A. McIntyre, A. C. Mix, J. J. Morlet, N. G. Pisias, W. L. Prell, and N. J. Shackleton (1984), The orbital theory of Pleistocene climate: Support from a revised chronology of the marine δ^{18}O record, in *Milankovitch and Climate*, Part 1, edited by A. Berger et al., pp. 269–305, D. Reidel Publishing Co., Dordrecht, Netherlands.
Jacobs, J. A. (1994), *Reversals of the Earth's Magnetic Field*, pp. 69–125, Cambridge Univ. Press, N. Y.
Jin, C. S., and Q. S. Liu (2010), Reliability of the natural remanent magnetization recorded in Chinese loess, *J. Geophys. Res.*, *115*, B04103, doi:10.1029/2009JB006703.
Jin, C. S., and Q. S. Liu (2011a), Revisiting the stratigraphic position of the Matuyama-Brunhes geomagnetic polarity boundary in Chinese loess, *Palaeogeogr. Palaeoclimatol. Palaeoecol.*, *299*(1–2), 309–317.
Jin, C. S., and Q. S. Liu (2011b), Remagnetization mechanism and a new age model for L_9 in Chinese loess, *Phys. Earth Planet. Inter.*, *187*(3–4), 261–275.
Kukla, G. (1987), Loess stratigraphy in central China, *Quat. Sci. Rev.*, *6*, 191–219.
Kukla, G., and Z. S. An (1989), Loess stratigraphy in central China, *Palaeogeogr. Palaeoclimatol. Palaeoecol.*, *72*, 203–225.
Kukla, G., F. Heller, X. M. Liu, T. C. Xu, T. S. Liu, and Z. S. An (1988), Pleistocene climates in China dated by magnetic-susceptibility, *Geology*, *16*(9), 811–814, doi:10.1130/0091-7613.
Lisiecki, L. E., and M. E. Raymo (2005), A Pliocene-Pleistocene stack of 57 globally distributed benthic δ^{18}O records, *Paleoceanography*, *20*, PA1003, doi:10.1029/2004PA001071.
Liu, Q. S., A. P. Roberts, E. J. Rohling, R. X. Zhu, and Y. B. Sun (2008), Post-depositional remanent magnetization lock-in and the location of the Matuyama-Brunhes geomagnetic reversal boundary in marine and Chinese loess sequences, *Earth Planet. Sci. Lett.*, *275*(1–2), 102–110.
Liu, T. S. (1985), *Loess and the Environment*, pp. 1–481, China Ocean Press, Beijing.
Liu, T. S. (1966), *Composition and Texture of Loess*, 132 p., Science, Beijing.
Liu, T. S., and Z. L. Ding (1998), Chinese loess and the paleomonsoon, *Annu. Rev. Earth Planet. Sci.*, *26*, 111–145.
Liu, T. S., Z. L. Ding, and N. Rutter (1999), Comparison of Milankovitch periods between continental loess and deep sea records over the last 2.5 Ma, *Quat. Sci. Rev.*, *18*, 1205–1212.
Liu, W. M., L. Y. Zhang, and J. M Sun (2010), High resolution magnetostratigraphy of the Luochuan loess-paleosol sequence in the central Chinese Loess Plateau, *Chin. J. Geophys.*, *53*, 888–894.
Liu, X. M., T. S. Liu, T. C. Xu, C. Liu, and M. Y. Chen (1988), The Chinese loess in Xifeng, I. The preliminary study on magnetostratigraphy of a loess profile in Xifeng area, Gansu Province, *Geophys. J.*, *92*, 345–348.
Lu, H. Y., X. D. Liu, F. Q. Zhang, Z. S. An, and J. Dodson (1999), Astronomical calibration of loess–paleosol deposits at Luochuan, central Chinese loess plateau, *Paleogeogr. Paleoclimatol. Paleoecol.*, *154*, 237–246.
Meeril, R., M. McElhinny, and P. McFadden (1996), *The Magnetic Field of the Earth: Paleomagnetism, the Core, and the Deep Mantle*, pp. 98–203, Academic, San Diego, Calif.
Oda, H., H. Shibuya, and V. Hsu (2000), Palaeomagnetic records of the Brunhes/Matuyama polarity transition from ODP Leg 124 (Celebes and Sulu seas), *Geophys. J. Int.*, *142*, 319–338.
Okada, M., and N. Niitsuma (1989), Detailed paleomagnetic records during the Brunhes-Matuyama geomagnetic reversal, and a direct determination of depth lag for magnetization in marine sediments, *Phys. Earth Planet. Inter.*, *56*, 133–150.
Porter, S. C., and Z. S. An (1995), Correlation between climate events in the North Atlantic and China during the last glaciation, *Nature*, *375*, 305–308.
Qiang, X. K., et al. (2011), New eolian red clay sequence on the western Chinese Loess Plateau linked to onset of Asian desertification about 25 Ma ago, *Sci. China Earth Sci.*, *54*, 136–144.
Rutter, N. W., Z. L. Ding, M. E. Evans, and Y. C. Wang (1990), Magnetostratigraphy of the Baoji loess-paleosol section in the north-central China Loess Plateau, *Quat. Int.*, *7*, 97–102, doi:10.1016/1040-6182 (90)90043-4.
Rutter, N., Z. L. Ding, M. E. Evans, and T. S. Liu (1991), Baoji-type pedostratigraphic section, loess plateau, north-central China, *Quat. Sci. Rev.*, *10*, 1–22.
Spassov, S., F. Heller, M. E. Evans, L. P. Yue, and Z. L. Ding (2001), The Matuyama-Brunhes geomagnetic polarity transition at Lingtai and Baoji, Chinese Loess Plateau, *Phys. Chem. Earth*, *26*, 899–904.
Spassov, S., F. Heller, M. E. Evans, L. P. Yue, and T. Dobeneck (2003), A lock-in model for the complex Matuyama-Brunhes boundary record of the loess/palaeosol sequence at Lingtai (Central Chinese Loess Plateau), *Geophys. J. Int.*, *155*(2), 350–366.
Suganuma, Y., Y. Yokoyama, T. Yamazaki, K. Kawamura, C. S. Horng, and H. Matsuzaki (2010), ^{10}Be evidence for delayed acquisition of remanent magnetization in marine sediments: Implication for a new age for the Matuyama-Brunhes boundary, *Earth Planet. Sci. Lett.*, *296*, 443–450.

Suganuma, Y., J. Okuno, D. Heslop, A. P. Roberts, T. Yamazaki, and Y. Yokoyama (2011), Post-depositional remanent magnetization lock-in for marine sediments deduced from ^{10}Be and paleomagnetic records through the Matuyama-Brunhes boundary, *Earth Planet. Sci. Lett.*, *311*, 39–52.

Sun, D. H., J. Shaw, Z. S. An, and T. Rolph (1993), Matuyama/Brunhes (M/B) transition recorded in Chinese loess, *J. Geomagn. Geoelectr.*, *45*, 319–330.

Sun, D. H., J. Shaw, Z. S. An, M. Y. Cheng, and L. P. Yue (1998a), Magnetostratigraphy and paleoclimatic interpretation of a continuous 7.2 Ma Late Cenozoic eolian sediments from the Chinese Loess Plateau, *Geophys. Res. Lett.*, *25*, 85–88.

Sun, D. H., Z. S. An, J. Shaw, J. Bloemendal, and Y. B. Sun (1998b), Magnetostratigraphy and palaeoclimatic significance of late Tertiary aeolian sequences in the Chinese Loess Plateau, *Geophys. J. Int.*, *134*, 207–212.

Sun, J. M., and T. S. Liu (2000), Stratigraphic evidence for the uplift of the Tibetan Plateau between 1.1 and 0.9 Myr ago, *Quat. Res.*, *54*, 309–320.

Sun, Y. B., S. C. Clemens, Z. S. An, and Z. W. Yu (2006a), Astronomical timescale and palaeoclimatic implication of stacked 3.6-Myr monsoon records from the Chinese Loess Plateau, *Quat. Sci. Rev.*, *25*, 33–48.

Sun, Y. B., J. Chen, S. C. Clemens, Q. S. Liu, J. F. Ji, and R. Tada (2006b), East Asian monsoon variability over the last seven glacial cycles recorded by a loess sequence from the northwestern Chinese Loess Plateau, *Geochem. Geophys. Geosyst.*, *7*, Q12Q02, doi:10.1029/2006GC001287.

Sun, Y. B., H. Y. Lu, and Z. S. An (2006c), Grain size of loess, palaeosol and Red Clay deposits on the Chinese Loess Plateau: Significance for understanding pedogenic alteration and palaeomonsoon evolution, *Palaeogeogr. Palaeoclimatol. Palaeoecol.*, *241*(1), 129–138.

Sun, Y. B., X. K. Qiang, Q. S. Liu, J. Bloemendal, and X. L. Wang (2013), Timing and lock-in effect of the Laschamp geomagnetic excursion in Chinese loess, *Geochem. Geophys. Geosyst.*, *14*, 4952–4961, doi:10.1002/2013GC004828.

Tauxe, L., T. Herbert, N. J. Shackleton, and Y. S. Kok (1996), Astronomical calibration of the Matuyama-Brunhes boundary: Consequences for magnetic remanence acquisition in marine carbonates and the Asian loess sequences, *Earth Planet. Sci. Lett.*, *140*(1–4), 133–146.

Vandenberghe, J., Z. S. An, G. Nugtern, H. Y. Lu, and K. V. Huissteden (1997), New absolute time scale for the Quaternary climate in the Chinese loess region by grain-size analysis, *Geology*, *25*, 35–38.

Wang, R. H., and R. Løvlie (2010), Subaerial and subaqueous deposition of loess: Experimental assessment of detrital remanent magnetization in Chinese loess, *Earth Planet. Sci. Lett.*, *298*, 394–404.

Wang, X. S., Z. Y. Yang, R. Løvlie, Z. M. Sun, and J. L. Pei (2006), A magnetostratigraphic reassessment of correlation between Chinese loess and marine oxygen isotope records over the last 1.1 Ma, *Phys. Earth Planet. Inter.*, *159*, 109–117.

Wang, X. S., R. Løvlie, Y. Chen, Z. Y. Yang, J. L. Pei, and L. Tang (2014), The Matuyama-Brunhes polarity reversal in four Chinese loess records: High-fidelity recording of geomagnetic field behavior or a less than reliable chronostratigraphic marker?, *Quat. Sci. Rev.*, *101*, 61–76.

Wang, Y. Q., M. A. Shao, Z. P. Liu, and R. Horton (2013), Regional-scale variation and distribution patterns of soil saturated hydraulic conductivities in surface and subsurface layers in the loessial soils of China, *J. Hydrol.*, *487*, 13–23.

Xiao, J. L., and Z. S. An (1999), Three large shifts in East Asian monsoon circulation indicated by loess-paleosol sequences in China and late Cenozoic deposits in Japan, *Paleogeogr. Paleoclimatol. Paleoecol.*, *154*, 179–189.

Yamazaki, T., and H. Oda (2001), A Brunhes-Matuyama polarity transition record from anoxic sediments in the South Atlantic (Ocean Drilling Program Hole 1082C), *Earth Planets Space*, *53*, 817–827.

Yang, S., and Z. Ding (2008), Advance-retreat history of the East-Asian summer monsoon rainfall belt over northern China during the last two glacial–interglacial cycles, *Earth Planet. Sci. Lett.*, *274*, 499–510.

Yang, T. S., M. Hyodo, Z. Y. Yang, and J. L. Fu (2004), Evidence for the Kamikatsura and Santa Rosa excursions recorded in eolian deposits from the southern Chinese Loess Plateau, *J. Geophys. Res.*, *109*, B12105, doi:10.1029/2004JB002966.

Yang, T. S., M. Hyodo, Z. Y. Yang, H. D. Li, and M. Maeda (2010), Multiple rapid polarity swings during the Matuyama-Brunhes transition from two high-resolution loess-paleosol records, *J. Geophys. Res.*, *115*, B05101, doi:10.1029/2009JB006301.

Yang, T. S., et al. (2014), High-frequency polarity swings during the Gauss-Matuyama reversal from Baoji loess sediment, *Sci. China Earth Sci.*, *57*(8), 1929–1943, doi:10.1007/s11430-014-4825-4.

Yu, Z. W., and Z. L. Ding (1998), An automatic orbital tuning method for the Paleoclimate records. *Geophys. Res. Lett.*, *25*, 4525–4528.

Zhao, X., and A. P. Roberts (2010), How does Chinese loess become magnetized?, *Earth Planet. Sci. Lett.*, *292*, 112–122.

Zhou, L. P., and N. J. Shackleton (1999), Misleading positions of geomagnetic reversal boundaries in Eurasian loess and implications for correlation between continental and marine sedimentary sequences, *Earth Planet. Sci. Lett.*, *168*(1–2), 117–130.

Zhou, W. J., J. W. Beck, X. H. Kong, Z. S. An, X. K. Qiang, Z. K. Wu, F. Xian, and H. Ao (2014), Timing of the Brunhes-Matuyama magnetic polarity reversal in Chinese loess using ^{10}Be, *Geology*, *42*, 467–470.

Zhu, R. X., Z. L. Ding, H. N. Wu, B. C. Huang, and J. Liu (1993), Details of magnetic polarity transition recorded in Chinese loess section, *J. Geomagn. Geoelectr.*, *45*, 289–299.

Zhu, R. X., C. Laj, and A. Mazaud (1994), The Matuyama-Brunhes and Upper Jaramillo transitions recorded in a loess section at Weinan, north-central China, *Earth Planet. Sci. Lett.*, *125*(1–4), 143–158.

Zhu, R. X., Y. X. Pan, B. Guo, and Q. S. Liu (1998), A recording phase lag between ocean and continent climate changes: Constrained by the Matuyama/Brunhes polarity boundary, *Chin. Sci. Bull.*, *43*, 1593–1598.

Zhu, R. X., R. Zhang, C. L. Deng, Y. X. Pan, Q. S. Liu, and Y. B. Sun (2007), Are Chinese loess deposits essentially continuous?, *Geophys. Res. Lett.*, *34*, L17306, doi:10.1029/2007GL030591.